



Interactive mold design for paediatric lower airway manikin manufacturing: a feasibility study

Luca Puggelli¹ · Rocco Furferi¹ · Yary Volpe¹

Received: 28 July 2022 / Accepted: 14 April 2023
© The Author(s) 2023

Abstract

According to previous research, shore 40 A casting silicone is currently one of the more suitable materials for simulating the physical behavior of the airways in medicine simulation. This is essential to attain high-fidelity manikins that can perfectly mimic the simulated anatomic region, not just geometrically, but also in terms of haptic feedback. Due to the geometrical complexity of the tracheo-bronchial tree, mold design is a difficult and time-consuming process. An interactive modeling procedure for modeling mold parts for tracheo-bronchial tree casting is proposed in this paper, with the purpose of reducing modeling time without compromising quality. Following the definition of a standard modeling procedure, this was implemented in the Matlab language by using an IGES and STL editing toolbox. By using the interactive procedure it is possible to reduce the time required for virtual modeling from several hours to less than 1 min. Given this preliminary result, the proposed procedure will be further tested and developed in the near future, with the possibility of automating other lower airway modeling steps, such as vent generation and mounting holes/pins.

Keywords Airway simulation · 3D modelling · Mold casting · Interactive design

1 Introduction

In the last decade, the use of high-fidelity life-size simulation manikins has grown exponentially in clinical practice, both for training and for pre-surgery planning applications. The benefits that can be achieved by using these technologies are incredibly relevant in many ways. For what concerns training, the use of manikins proved to be much more effective than the traditional technique, which consists of direct practice on real-world settings under expert supervision. In fact, it has been observed that the everyday exercise of routine procedures on realistic anatomical models, possibly with an increasing difficulty level, ensures greater patient safety as the risk of complications is reduced [1, 2].

Referring to pre-surgery planning, the availability of patient-specific simulators, which are 3D models developed based on the anatomy of a single patient, enables skilled surgeons to improve the surgery plan before entering the operating room. As a result, this enables both simulation and investigation of multiple surgical techniques with the goal of determining the optimal one in terms of safety and effectiveness, while significantly reducing surgical times [3].

A key factor in both training and planning is that the simulator's properties closely mimic the ones of the actual body. In particular, the main aspects to be carefully reproduced in the manikin are geometric dimensions and haptic feedback (i.e. the touch feeling of the mannequin must be close to that of the real anatomy) [4, 5].

This is a critical factor in making the simulated experience truly realistic, despite its secondary relevance in many commercial simulators and specific research in the scientific literature [6–8]. As a matter of facts, anatomical structures are indeed composed of multiple organic materials, some of which are composed by fibres, with a consequent anisotropic behaviour. For this reason, in the scientific literature the mechanical characterization is generally referred to general structures and “equivalent” materials, whose mechanical

Rocco Furferi and Yary Volpe have contributed equally to this work.

✉ Luca Puggelli
luca.puggelli@unifi.it
Rocco Furferi
rocco.furferi@unifi.it
Yary Volpe
yary.volpe@unifi.it

¹ Department of Industrial Engineering, Univeristy of Florence, Via Di Santa Marta, 3, 50139 Florence, Italy

characteristics mimics the overall behaviour of the general anatomical structure or for the main substructure [9–11].

There are several airway simulators on the market, but the majority of them are intended for adult patients and are not appropriate for paediatric medicine, with only a few having a high degree of verosimilarity with real anatomy. Only a small percentage of these replicate complex clinical pictures (e.g. tracheomalacia), the Meyer Children Hospital (Florence, Italy) anesthesiology team believes they are still overly simplified in comparison to reality.

To partially confront with this issue, the typical workflow adopted by bioengineers starts from the retrieval and virtual 3D model reconstruction of the internal anatomy by analysing diagnostic images, mainly obtained by means of *Computed Tomography* (CT) and *Magnetic Resonance Imaging* (MRI). The accuracy of CT-based 3D reconstruction has been validated in previous studies [12], in which an average accuracy error of 0.1 mm has been measured in a set of 3D reconstructions obtained from CT scans. Once the virtual shape of the manikin is opportunely retrieved, the next step is to realize the physical replica of the anatomic region by means of advanced computer-based manufacturing techniques, such as *Additive Manufacturing* (AM). Unfortunately, despite the increasing variability of 3D-printable materials, with several typologies of soluble support materials and a list of rubber-like model materials with varying hardness (which could be used to 3D-print to replicate soft anatomical tissues), direct 3D-printing cannot always achieve the desired haptic feedback, resulting too stiff and hard to correctly mimic the real tissue. This issue is more evident in case of paediatric patients, since tissues (and lower-airways anatomies in particular) are softer than in adults.

Not by chance, in a previous investigation [13], several materials have been tested with the help of a team of physicians of *Meyer Children Hospital* (Florence, Italy) in order to detect which one better reproduces the actual anatomic feedback of lower airways anatomies. Shore 40A silicone [14] proved to be the most suitable for creating the replicas, while all 3D printed materials were considered excessively hard and stiff. In particular, a specific investigation on paediatric tracheal stiffness has been carried out in the aforementioned literature paper, taking into consideration the lowest values for adult tracheal cartilage retrieved in other works (i.e. varying in the range 1–3.3 MPa). The choice of considering cartilage stiffness is motivated by the fact that cartilage rings are the structure responsible to maintain the trachea open during respiration, preventing collapse. Such values are hardly obtainable using direct 3D printing. Quite the reverse, 40 Shore A silicone has an adequate stiffness (approximately equal to 3 MPa). As mentioned before, the possibility of realising the airways' replica by means of direct 3D printing is therefore not recommended. Such a method should be replaced by an aptly devised mould casting production

techniques, despite the fact that mould design is not simple and requires longer modelling timings. This sums up with the fact that the expected successive manufacturing is typically limited to few replicas but characterized by several items (i.e. different airways' geometry). It has, indeed, to be taken into account that ideally 20 replicas for 10–15 different items are required to build a consistent dataset of case studies for training and pre-planning.

As stated by the aforementioned concerns, the optimization of the modelling phase of the mould-based production of lower airways is still a key issue in paediatric medicine and the main drawbacks related to the replica manufacturing, hinted above, should be confronted with. Accordingly, the main aim of the present paper is to provide a preliminary interactive method capable of carrying out a semi-automated mould manufacturing to be used for creating replicas, which reliably resemble the actual anatomy of interest. Such replicas are modelled and produced with the intention of embedding them in an under continuous development manikin, utilized for training and surgery planning of procedures on lower airways in the paediatric field.

The paper is structured as follows: in Sect. 2, a brief introduction to lower airway anatomy is given together with the main required characteristics for the manikin. In Sect. 3 a standard modelling process is proposed with the aim of translating it into an interactive procedure according to the workflow proposed in Sect. 4. Finally, the first results obtained with the implemented procedure and future development are discussed in the conclusion.

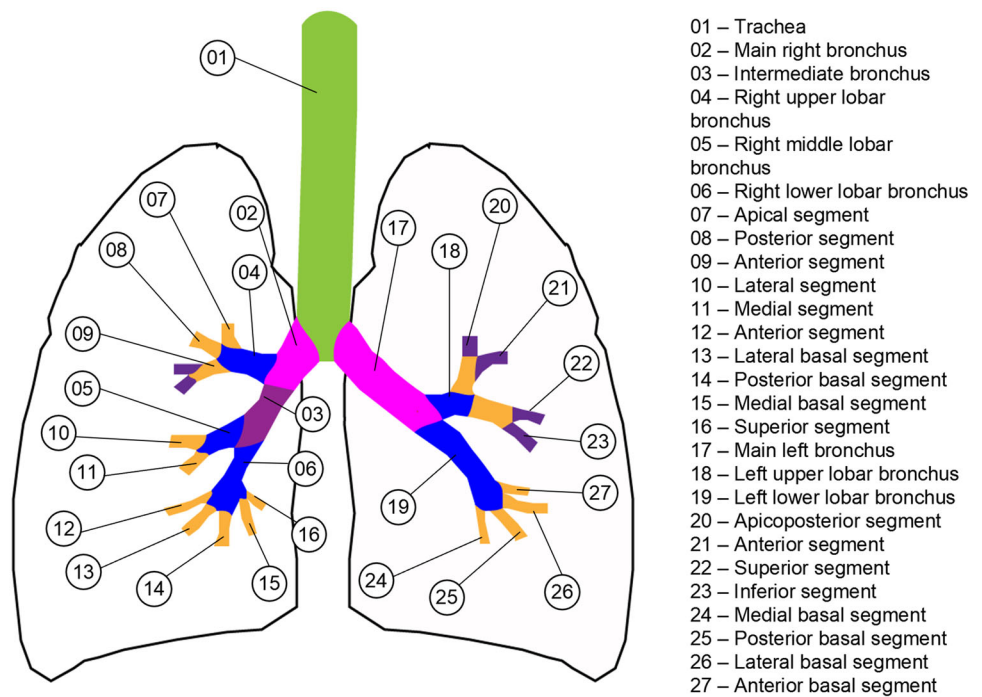
2 Lower airway's anatomy and manikin characteristics

As mentioned before, before proceeding with the description of the mould's standard modelling process and its automation, this Section provides a brief introduction to the characteristics of the anatomical districts of interest. Successively, a description of the lower airways manikin's layout is provided and the principal issues related to its manufacturing are briefly introduced and discussed.

2.1 Lower airways' anatomy

As widely recognized, the respiratory tract consists of two distinct sections: upper and lower airways. The upper airways, or upper respiratory tract, starts from the nose and ends in the upper portion of the larynx, above the vocal folds (cords). The lower airways or lower respiratory tract includes the portion of the larynx below the vocal folds, trachea, bronchi and bronchioles. In this work, the lungs region is not taken into account for modelling and prototyping, therefore it is not included in the manikin development.

Fig. 1 Schematic anterior view of lower airways: trachea (green), primary bronchi (pink/dark pink), secondary bronchi (blue), tertiary bronchi (yellow), bronchioles (purple)



The main structure of the lower airways (see Fig. 1) is the tracheobronchial tree (successively referred as TBT), which comprises trachea (i.e. the main vertical trait), main bronchi (left and right), lobar bronchi (or secondary, three on the right and two on the left), segmental bronchi (or tertiary) [15].

Trachea wall has many layers: mucosa, submucosa and adventitia, plus a layer of hyaline cartilage. Mucosa is the inner layer, surrounded by submucosa and a number of C-shaped rings of hyaline cartilage. The outermost layer is composed by connective tissue (adventia). The internal cavity of the TBT is called lumen. Trachea begins right below vocal chords and bifurcates into the right and left main stem bronchi. The downward and backward projection of the last tracheal cartilage is the carina, which marks the bifurcation point.

2.2 Lower airways' manikin characteristics

Referring to the classification expressed in the previous subsection, the lower airways' section of the manikin, which must be designed, has to include trachea, main bronchi and secondary bronchi. Tertiary bronchi will be partially realized in their initial section. The lower airways' part is attached to the head of the manikin by means of a locking system, whose details are not discussed in this paper (see Fig. 2).

The initial part of the TBT consists (on the outside) of a 5 mm thick disk ("connection disk") that matches with the inner geometry of the locking system.

For what concerns the modelling process of the TBT part, this is carried out by means of the following six steps procedure, described in the following paragraphs:

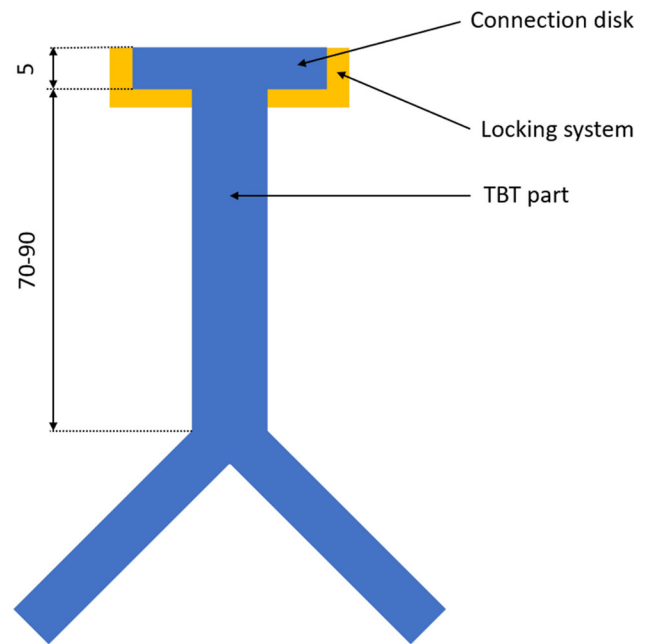


Fig. 2 Layout of the lower airways' manikin, including tracheobronchial tree and locking system

1. Lumen 3D geometry reconstruction
2. *TBT part* definition
3. *Connection disk* definition and alignment
4. Boolean merge *TBT part* + *connection disk* = *TBT gross-shape*
5. Lumen loft = *complete lumen*
6. Boolean subtraction (*TBT gross-shape* - *complete lumen*)

The lumen geometry is obtained from diagnostic images (generally by means of CT), by using *Mimics*[®] software. A common procedure starts with the 3D segmentation of the region of interest on each slice of the *DICOM* file. In our case study, the medical images has been obtained by means of *Philips Brilliance 64* CT spiral scanner, with 0,8 mm slice thickness 100 kV tube potential and 200 mAs tube current (for privacy reasons, no further information can be disclosed). The obtained 3D mask is defined in the discrete voxel domain (volume pixel) and coincides with a first 3D model of the anatomy. Successively, the 3D polygonal model is obtained by applying *marching cube algorithm* (or one of its variations).

Once the lumen 3D polygonal geometry has been defined, it is possible to proceed with the *TBT part* design. This modeling phase is performed by means of *Geomagic Design X* software. *TBT part* is obtained as the 2 mm outer offset of the lumen. This specific offset value will ensure 2 mm TBT walls thickness in the final piece, which has been defined according to physicians staff of *Meyer Children Hospital*. The *connection disk* is a standard interface for this specific manikin, which allows to attach different TBT models to the manikin's head by means of a specifically designed locking system. Disk's shape and dimensions are then defined a-priori, and its position coincides with the upper end of the tracheal trait of TBT. Once connection disk and TBT are aligned, they are merged and *TBT gross shape* is obtained. Successively, lumen is extended in the upper part (i.e. on the tracheal trait) with a 5 mm loft, which has been previously discussed and the *complete lumen* is obtained. Finally, *TBT gross-shape* is subtracted by the *complete lumen*, resulting into the definitive TBT part.

2.3 Mold casting tracheo-bronchial tree

As mentioned in the introductory section, all the most suitable material to create the manikin airways' parts is silicone. To this purpose, the elective manufacturing process is mold casting. Due to the particular geometry of the anatomical part to be cast, AM technologies are the best option to create the mold. This is a tricky task, due to the complexity of branched geometry. In fact, such a geometry prevents the extraction of the core used to realize the lumen once the silicone has solidified, even by considering the possibility of either breaking away each core's branch or sub-dividing the core in multiple separable components. In the first case, the extraction of core fragments is practically unfeasible since several of them may result stuck into the silicone mass. In the second case, there is a high probability of silicone seeping into the gaps between components, making extraction impossible and obstructing the lumen. These issues have been solved by realizing the core in a dissolvable material, available for 3D printing. One of the most common is PVA (*Poly-Vinyl-Alcohol*), which

dissolves in water and it is used both as model and support material in FDM 3D printers. An alternative, which is the preferred solution in this work, is the use of *Stratasys*[®] *SR30*[™], a support material available for *Fortus*[®] *Stratasys* FDM 3D printers.

Another important issue for mold design phase is related to branches' directions. If all branches are approximated to straight traits, they did not lay on the same plane. Moreover, the most extended branches (trachea and main bronchi) are far from being straight in some cases, especially in case of malformation. Consequently, multiple extraction planes must be retrieved, and the mold has to be subdivided in more than two parts. For this reason, one of the main aims of this work is to provide a standard procedure to design each mold's part in CAD environment, starting from the lumen geometry. This manual procedure lays the foundation for a subsequent interactive automation, as described in the reminder of the paper. Finally, each terminal branch's cavity must be blind, to avoid the environmental light to enter the manikin's airways. This means that the mold's core will be surrounded by silicone during the casting, except for the trachea side. Therefore, casting must be performed with the trachea in vertical position and the core must be equipped with a plate on the trachea side to allow correct positioning in the mold.

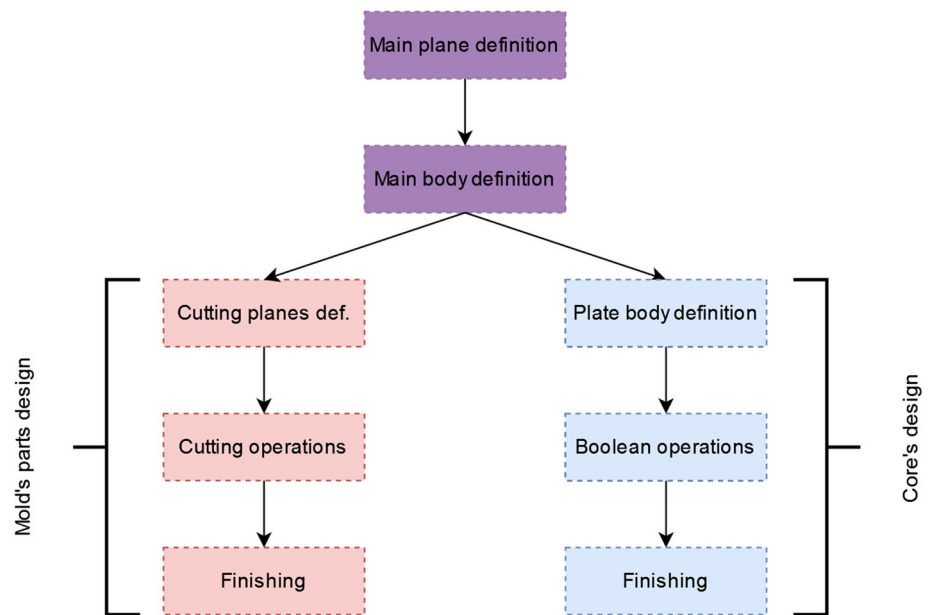
3 Mold design: definition of a standard modelling procedure

3.1 Input data and procedure workflow

Focusing the attention on mold design, the idea is to exploit auxiliary parts that have been defined to model TBT manikin's part, *gross shape* and *complete lumen* in particular. The first one will be used to model mold's cavity to obtain the external shape of the TBT. The second will be used to model the internal core, to obtain the lumen, i.e. the internal cavity of the TBT.

For what concerns extraction planes definition, the idea is to use information about branches' directions. In this way, it would be possible to "follow" branches with the planes set and obtain a proper sub-division of the mold. This can be done using the lumen *centerline*, i.e. the curve that passes through the center of each airways' cross-section. In the continuous domain, *centerline* retrieval can result tricky while results may be affected by unwanted phenomena (e.g. loops formation). *Skeletoning* algorithms, which are used to reduce a volume (or a 2D shape) to its skeleton and - in the case presented in this work - to reduce airways' volume to its centerline, are optimized to operate in discrete domain (2D raster images, in particular). Luckily, *Mimics*[®] includes *Centerline Tool*, a tool dedicated to the automatically *centerline*

Fig. 3 Mold's and core's parts modelling procedure workflow



retrieval of tubular anatomical regions in the voxel domain of the *DICOM* file.

The input data set is now complete, and it is possible to move on to the definition of the standard modeling technique. The general idea is to obtain each mold's part geometry by means of cut operation on a *main body*. The modelling procedure is depicted in Fig. 3.

The workflow consists of two preliminary steps used for defining the *main plane* and the *main body*, which will be used for both core and mold modelling. Then, the design of mold and core follows different parallel steps, which are described in the next subsections.

3.2 Main plane and main body definition

The first two steps of the procedure summarized in Fig. 3 are suitable to design both mold's parts and core. The relevant steps for the definition of main plane and main body are described in the following sections.

3.2.1 Main plane definition

The first step consists of the definition of the main plane, which approximately coincides with *xz* plane according to [16]. This plane is the one that ideally approximates the single extraction plane and coincides with the plane that best-fit the *centerline*. This plane is used as a reference for both *main body* and *cutting planes* definition.

3.2.2 Main body definition

The *main body* is obtained as the extrusion of a sketch drawn on the *main plane*. Its overall volume must include TBT part

and should be large enough to offer the possibility of hosting pins and holes for mold's parts positioning (these features will be realized in the finishing phase). In this paper, this sketch can be simplified to a rectangle.

Referring to Fig. 4, *centerline* is projected into the main plane (*Projected Centerline - PCL*). A and B points are defined as the first and last point of PCL corresponding to trachea. Successively, the *bounding box* of PCL whose side is parallel to AB is retrieved. The rectangle is obtained as the outer 5 mm offset of this *bounding box*.

To define the depth of the extrusion upwards and inwards versus the *main plane*, the maximum distance of the *centerline* versus the *main plane* is evaluated in both directions, and it is extended by 5 mm. Eventually, by following the above steps, the *main body* is completely defined.

3.3 Mold's parts design

3.3.1 Cutting planes definition and cutting operations

The first step of the mold's part design aims at defining a set of *cutting planes* to subdivide the *main body* in a series of parts to allow the final piece extraction. As previously discussed, the idea is to exploit information coming from the *centerline*. In particular, by approximating the *centerline* to simplified tree graph it is possible to define a series of planes (or a polygonal surface) with the proper characteristics. One possible strategy is to triangulate these points together with the rectangle vertices on the *main plane*, maintaining tree graph edges. In this way, each triangle in the 3D space corresponds to a planar surface, while all the triangles compose a polygonal mesh. This mesh fits the requirements since it

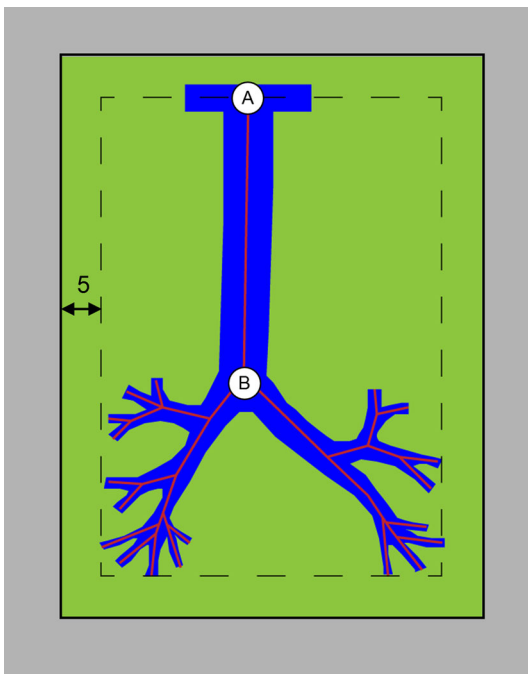


Fig. 4 Centerline's bounding-box and offset rectangle for mold's dimensions definition

follows the *centerline* (and so the TBT) and cuts the *main body* in two parts (see Fig. 5).

This strategy is generally effective for trachea and main bronchi. Unfortunately, this is not sufficient for successive branches. The main issue is related to the fact that 1) branches (and bifurcations) become denser and closer each other as they get smaller and 2) their directions become (highly) outward or inward pointing w.r.t. the *main plane*. This means that the angle between two adjacent triangles of the mesh becomes sharper, and this may result in the formation of undercuts along the direction of part extraction. To better understand this issue, some definitions must be taken. Let's call e an edge belonging to both *cutting mesh* and *centerline* and ep it's projection into the *main plane*. Let's now define Π plane, which is orthogonal to ep and passes through e midpoint (its position is not strictly necessary). At this point, it is possible to detect the intersection of both elements that share e with Π plane: ϑ is the angle between them and it needs to be checked to determine the part's extractability (see Fig. 6).

Approximating lumen cross-section to a r -radius circle and considering a maximum acceptable compression on silicone walls of 40%, since the thickness of the walls is 2 mm the minimum ϑ angle (see Fig. 7) that ensures the extraction from the mold is defined by the following equation:

$$\theta > \pi - 2 \arccos \left(\frac{r + 0.8}{r + 2} \right) \quad (1)$$

As a consequence, ϑ decreases, whereas lumen approximate radius increases. Excluding trachea and main bronchi,

which can be considered free from this issue, inner "radius" never exceeds 4 mm, corresponding to $\vartheta = 106^\circ$. Therefore this value can be considered as a general threshold, which is valid regardless of the inner radius. A careful examination of the mesh is necessary before moving on in sight of this observation, and certain countermeasures are required to solve this problem.

A straightforward solution is to subdivide the critical mold's part (part B, referring to Fig. 7) with a plane perpendicular to the main plane, passing through the *centerline* branch in which ϑ angle is below the threshold. This passage has to be repeated for each criticality. This operation, which has to be repeated for all critical branches/angles, resolves the issue in its entirety (Fig. 7).

In order to limit the number of mold's parts, the subdivision is applied only to the part that has ϑ -criticality (e.g., part B in Fig. 7). For a sake of clarity, let's make an example. Supposing that mold is divided by the mesh in part A and part B, and make this last affected by three ϑ -criticalities, as shown in red in Fig. 8A.

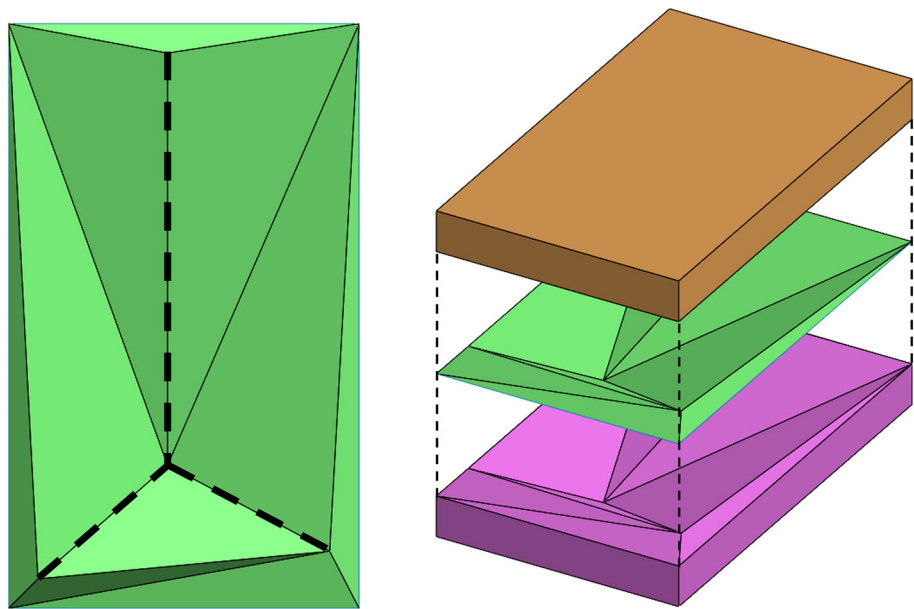
If the division operated by means of each one of the three resulting planes is applied to the whole part B, as a result a total of 7 subdivisions are obtained (see Fig. 8B). Otherwise, if the cut operation is applied only to the subdivision of interest, the total of parts is limited to 4, with a simplification in the successive designing step. In fact (see Fig. 8C), the first plane (red line) cuts part B in subdivisions 1 and 2, the second one (green line) cuts subdivision 2 in subdivisions 2 and 4 and the third one (blue line) cuts subdivision 3 in subdivisions 3 and 4.

3.3.2 Boolean operation and finishing

Once the mold's parts are retrieved, it is possible to move on with the Boolean subtraction of the lower airways part, in order to obtain the cavity for the silicone casting. This operation is quite straightforward since all parts are in the correct position (hence, no alignment is required). For what concerns finishing operations, three main tasks must be pursued: 1. Assembly check; 2. realization of a set of references for the correct positioning of mold's parts; 3. realization of vents.

Assembly check is carried out in order to verify a-priori if the assembly of mold's parts happens flawless. Two main aspects are investigated to this aim: absence of undercuts and correct clearance between parts. The first check aims at analyzing if the mold's part geometry design has been correctly retrieved. This is performed by visually analysing and (if required) measuring the 3D geometry and therefore requires an interaction with the user. The second aspect is related to contact surfaces, especially in the case of pin/hole coupling and convex edges. For pin/hole coupling, an allowance must be considered, depending on AM machine accuracy and pre-

Fig. 5 Main cutting mesh (green), centerline (dash line), mold's part A (orange) and part B (purple)



cision. In the case of using the *Statys Fortus 450mc* FDM printer, a 0.1 mm gap can be a good compromise to obtain a precise coupling. Convex edges must be chamfered or filleted ($0.5 \times 45^\circ$ is the selected value). Further, in order to lock mold's part in the correct position, a set of references (e.g. pins/holes) are needed. When possible, pins should be integrated in the parts' bodies. Moreover, through holes are preferable since support removal results easier and faster (also in the case of soluble support materials). Finally, vents are designed to allow air to easily escape from the mold.

3.4 Core design

Core design requires less modelling operations, compared to mold, and its principal phases are only briefly described, since they will be not object of the successive interactive automated phase. The main phase of the modelling, since lumen geometry is known, is the realization of the plate through which the core is coupled to the mold. It's shape is rectangular and its dimensions are defined referring to the *main body*. Basically, it is the result of a 5 mm extrusion of the -5 mm offset of the *main body* upper face. This is called *core's plate gross shape*.

Since casting operation will be performed with trachea in vertical position, the pouring basin must be located inside the core's plate. Its position and shape is defined on the basis of the lower airways part geometry. In particular, it must be in correspondence with the cavity corresponding to the disk of the lower airways part and it must not be coincident with the lumen (see Fig. 9). In order to maximise its dimension, to facilitate casting, it should be C-shaped. Finally, four through holes must be realized near the corners of the plate, to allow bolts connection between core and mold. Once all

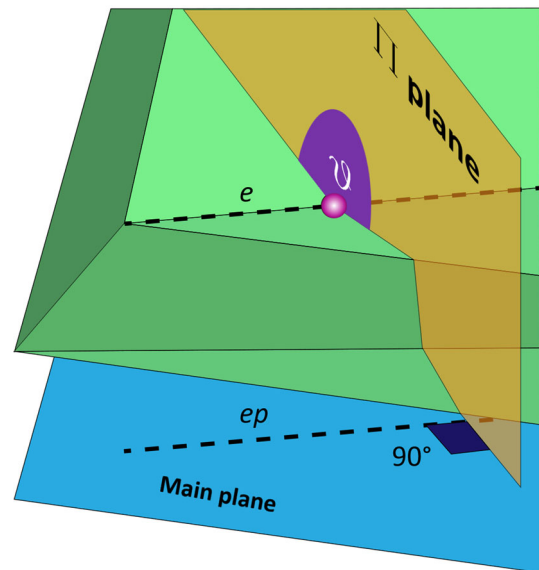


Fig. 6 Definition of e , ep , Π plane and ϑ angle

these operation are carried out, it is possible to proceed with the Boolean merge of the lumen and plate bodies.

4 Interactive procedure

In this chapter, the automated of the mold's parts design is introduced and described. All the procedure has been implemented in *Matlab*[®] coding environment. The automated is focused on four modelling steps, which are the definition of main plane, main body and cutting planes, and cutting operations. As mentioned above, finishing operation and core

Fig. 7 Critical angle in the main cutting mesh and proposed solution. Mold's parts (white), mold's core (orange), silicone part (yellow)

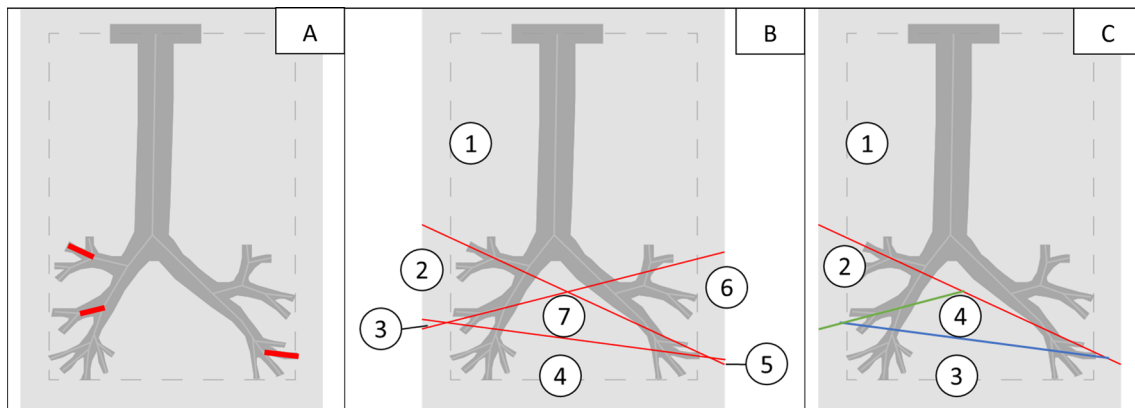
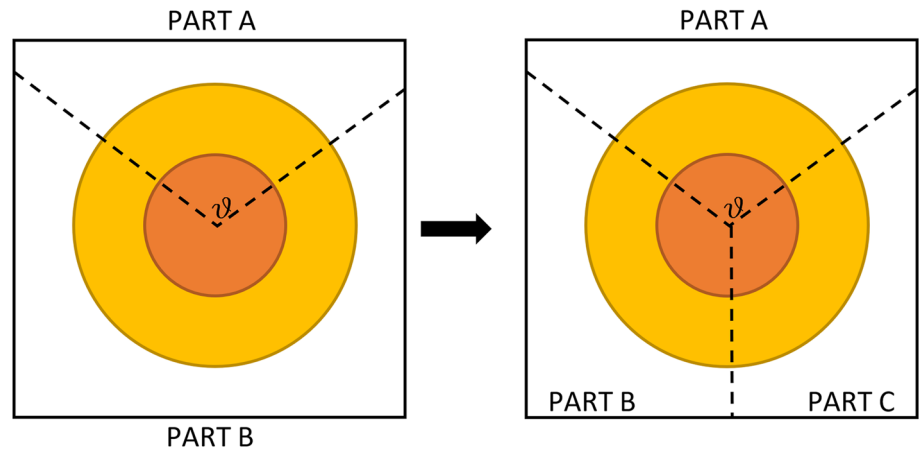


Fig. 8 Mold part subdivision due to ϑ criticalities

design are still meant to be carried out manually. In order to handle and edit STL files, *geom3d* toolbox is the used tool [17].

4.1 Preliminary operations

Before proceeding with the implementation of the modelling steps, some preliminary operations on *centerline* must be carried out in order to make it usable. Being exported as IGES file, the *centerline* can be imported in *Matlab*[®] workspace by using *IGES Toolbox* [18]. IGES files, and in particular curves, are approximated by a polynomial chain, which is expressed as an adjacent points couple list. In the case of a tree, all information about the starting point (i.e. the upper point of the tracheal trait), branches organization and the overall structure are not available and has to be retrieved in order to proceed with modelling operations. This step is carried out according to the method provided in [16]. In particular, starting point, ending points and bifurcation points are retrieved by analysing the point list, while the organized and sorted structure is retrieved by means of a *Matlab*[®] procedure specifically developed in the referenced paper. Such procedure also provide a simplified *centerline*, in which the

main points (i.e. starting point, ending points and bifurcation points) are preserved while the remaining part of the *centerline* is simplified by means of *Douglas-Peucker* algorithm [19] (a threshold value equal to 0.5 has been set, allowing an overall points reduction of about 90%). The simplified *centerline* is preferred, since it approximates the original geometry with a more-than sufficient accuracy for this application and it leads to a several advantages. The main one is that points are more distant each other, which leads to a more simple and clean main cutting mesh, since its elements will be less and larger. This makes finishing operations easier and faster. In the following, the *simplified centerline* will be simply referred to as *centerline*. In *Matlab*[®] workspace, *centerline* is a matrix in double precision format, in which the first 3 columns store x, y and z coordinates of its points while column 4 stores an id that indicates to which TBT branch it belongs.

4.2 Main plane and main body

Main plane is retrieved as the plane that best fits the *centerline* i.e. the one that better approximates its points, which are already stored in a matrix. To this purpose, the *fitPlane*

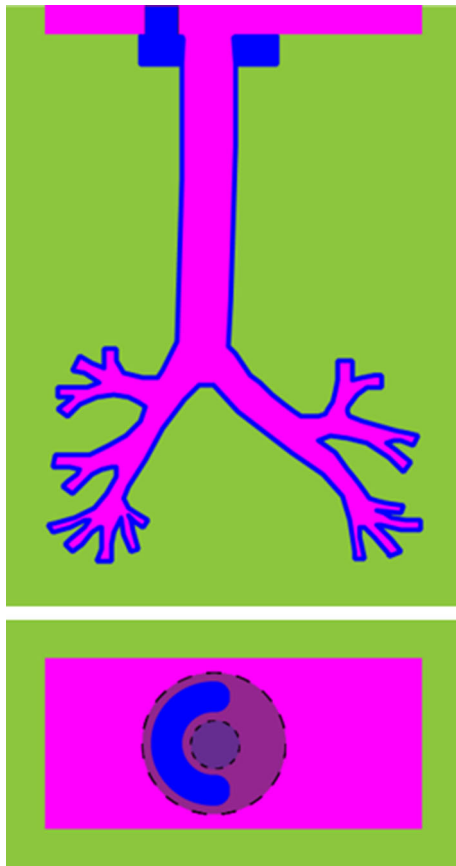


Fig. 9 Lateral and Top view of mold (green), core (pink) and cast silicone (blue), which includes the pouring basin

function is used. For what concerns *main body* design, some preliminary operations are required prior to retrieve its geometry. First, *centerline* points are rotated to align the *main plane* to the reference system's *xz*-plane. Let's call this transformation R1. Successively, *centerline* points are rotated to obtain tracheal direction parallel (i.e. the axis traced between the first and last tracheal points) to *z*-axis. Let's call this transformation R2. In this configuration, the 3D *bounding box* is retrieved by means of *boundingBox3d* function, in the form of:

$$[x_{max}, x_{min}, y_{max}, y_{min}, z_{max}, z_{min}] \quad (2)$$

Consequently, the 5 mm offset is obtained by adding 5 to max components and subtracting 5 mm to min components:

$$[x_{max} + 5, x_{min} - 5, y_{max} + 5, y_{min} - 5, z_{max} + 5, z_{min} - 5] \quad (3)$$

Since successive operation are performed with polygonal geometry, the bounding box is converted into the STL format. This has been directly obtained by using *boxToMesh* function, which is included in *geom3d* toolbox. The mesh vertices

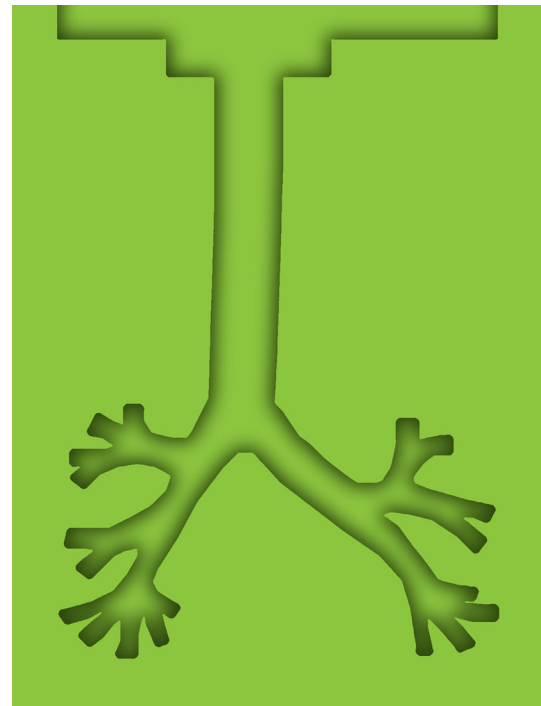


Fig. 10 Main body after Boolean subtraction of core's plate gross shape and TBT gross shape

are finally counter transformed by applying R2' and R1', which are respectively the counter rotations of R2 and R1. In this way, polygonal model's original orientation is reset. Finally, it is possible to proceed with Boolean operations, in which the *core's plate gross shape* and *TBT gross-shape* are subtracted from the *main body* (see Figs. 10 and 11).

4.3 Cutting planes definition

This section is dedicated to the definition of the *cutting mesh* and the (possible) *cutting planes* to avoid issues that have been previously discussed. The *cutting mesh* is obtained by means of *Delaunay triangulation* of a properly designed points grid and the *centerline* points [20].

A 5 mm spaced points grid is defined in the main plane as large as the main body cross-section on the main plane. Also *centerline* points are projected into the main plane, by using *projPointOnPlane* function. At this point, a threshold distance is defined as the median distance between adjacent projected *centerline* points. All grid points that falls within a distance from the projected *centerline* that is below the threshold, are deleted. The remaining grid points and projected *centerline* points are then triangulated. In the obtained mesh, the coordinates of the projected *centerline* are substituted by the *centerline* ones. In this way, the *cutting mesh* is completely defined (see Fig. 12).

To define the *cutting planes*, a *cutting mesh* analysis is performed to identify which couples of elements cause ϑ -

Fig. 11 Preliminary operations, main plane and main body definition flowchart

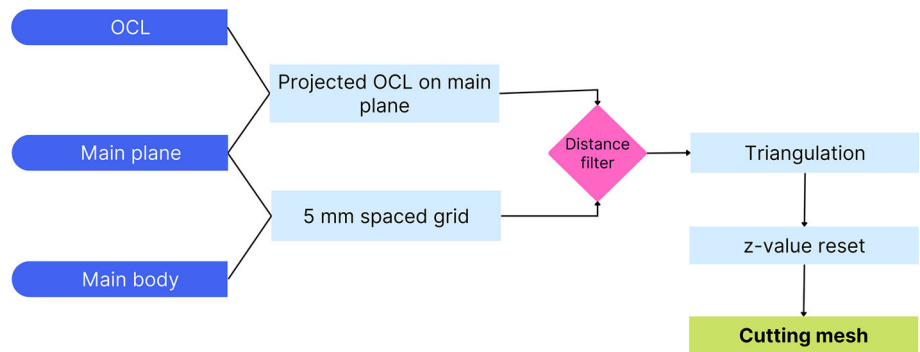
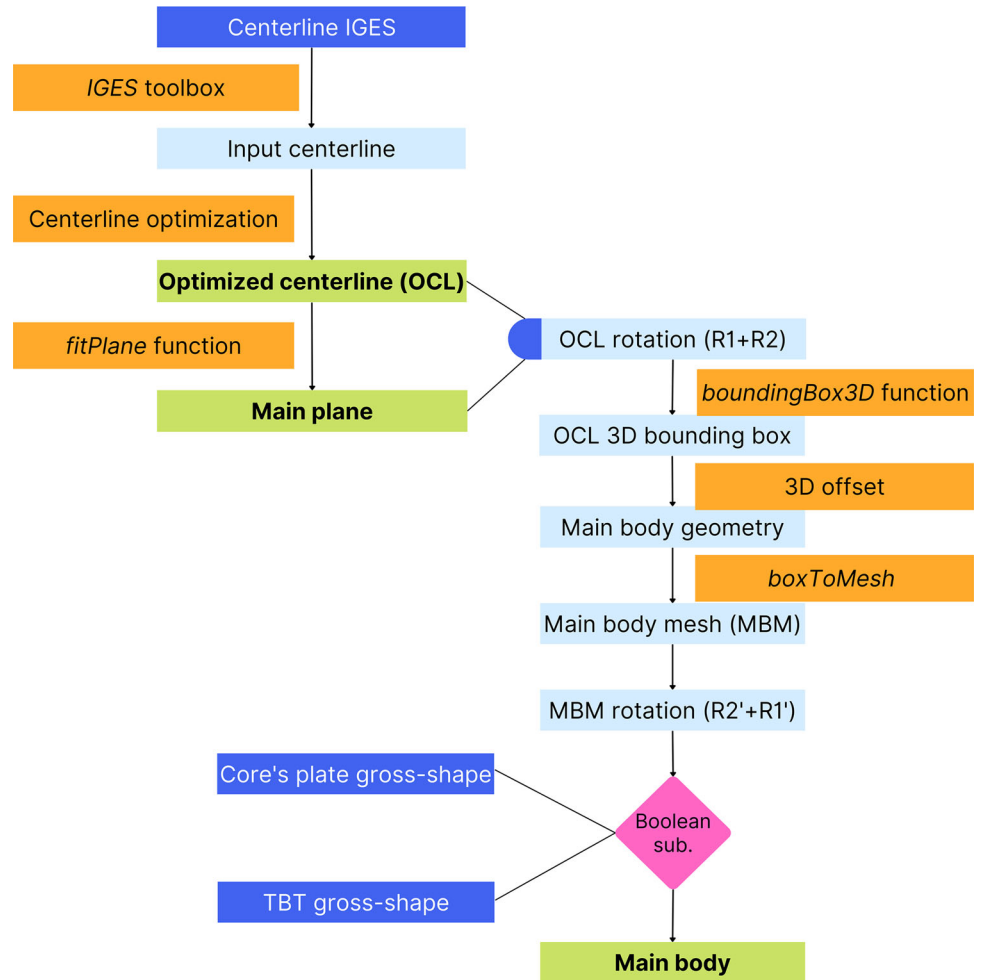


Fig. 12 Cutting mesh definition flowchart



criticality in correspondence with a *centerline* edge. This research is extended to all *centerline* branches, and it is performed by defining the Π plane for each branch, retrieve elements' intersections and evaluating the angle between them. If the resulting angle exceeds 106° threshold, the relative edge is considered critical and the lower part needs to be divided by a cutting plane. Conversely, if the angle results to be equal or above 254° (i.e. the complementary angle of 106°), the upper part needs to be divided.

The *cutting plane* definition is straightforward, since it will be the plane that is orthogonal to both the relative Π plane and the *main plane*, and that passes through the critical edge.

4.4 Boolean operations and cut

Cutting operations are performed sequentially and are limited to the subdivision of interest. At first, *main plane* is divided

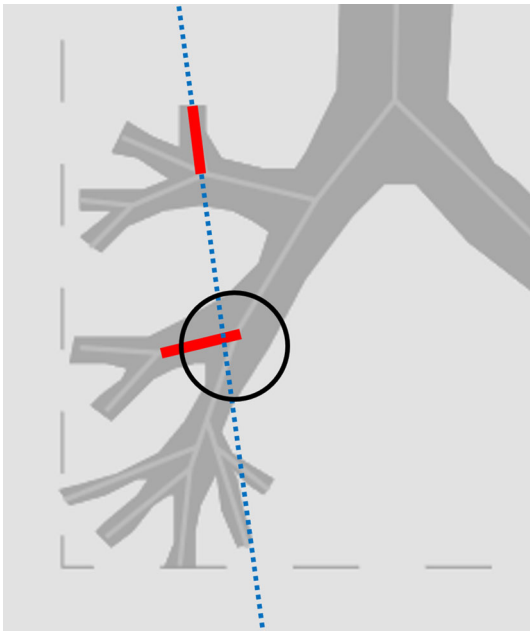


Fig. 13 Cutting plane that intersects a critical edge: this situation will lead to an over-subdivision of the mold

into A and B parts. Successive cutting-by-plane operations are arranged in A-part and B-part operations, according to ϑ angle analysis (performed in the previous step): in this way, cut will be done only where required. The same criteria are used, in accordance with what was previously described, to determine if a subsequent subdivision has to be reduced. In *Matlab*[®] environment, this is obtained by checking critical edges' positions. Starting from A-part, the first randomly selected cut will divide it into A1 and A2 parts. Since all critical edges' vertices are known, it is possible to select one of them and check its vertices' position. Two scenarios are possible: all vertices belong to the same subdivision or they belong to different ones. This last operation is not desirable since it would cause the division of two sub-parts instead of one (thus final sub-parts would be more in number). Actually, this situation only happens in a specific condition. Calling C and D two critical edges, this option takes place only if C cut is prior to D and if C-cut-plane and D critical edge are incident (see Fig. 13). To avoid it, an a-priori analysis is performed and, if this criticality emerges, the cutting order is changed.

Finally, cut operations are realized by means of specifically devised *Matlab*[®] functions, which are included in *geom3d* toolbox.

5 Conclusion

In this paper, it is proposed to automate a set of modeling steps for defining the mold's part geometry for casting a tracheo-bronchial tree manikin. The complete process still

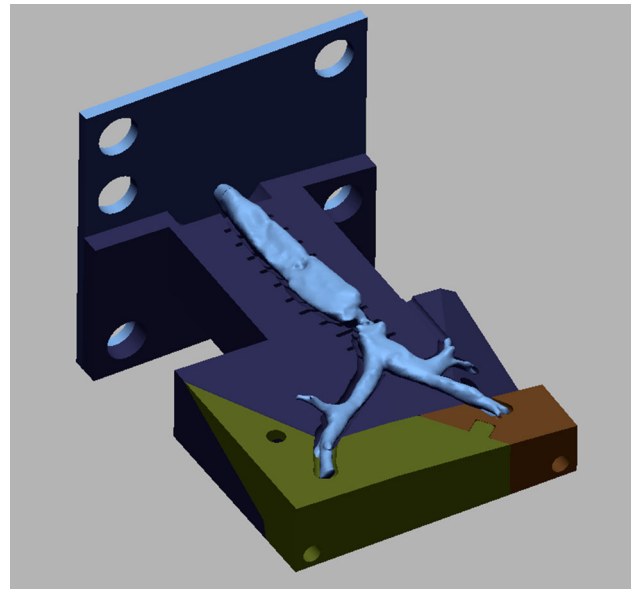


Fig. 14 Shape of mold's parts and mold's core, obtained with the proposed procedure in the case study

needs manual adjustments and refining, due to the complexity of the overall procedure and to the high variability in shape of real (and maybe malacic) lower airways. The interactive procedure has been implemented in *Matlab*[®] environment by using function toolboxes specifically devised to model and edit 3D polygonal geometries. The implemented procedure has been tested on a first case study, relative to a tracheo-bronchial tree of a patient in pediatric age affected by *tracheomalacia* (i.e. a collapse of the tracheal cartilage structure). The entire procedure took about 34'' to analyse the input data (tracheal STL geometry and tracheal centerline) and to complete the modelling steps. This represents a significant improvement respect to the manual modelling process, which requires much longer times (more than 1 h, depending on the complexity of the airways). Despite some minor adjustments on the mold's parts (e.g. the introduction of fillets on sharp edges to avoid "peaks" that could potentially cause interference between parts) the obtained result (visible in Fig. 14) is more than encouraging. In terms of model accuracy, this is influenced only by the cavity's geometry of the mold, which is not altered by the procedure and is modelled starting from medical images. As a result, whether the process is manual or follows the proposed procedure, the accuracy of the model (mold's cavity or final silicone tracheo-bronchial tree) is the same.

For this reason, the procedure will be deeper analyzed and tested on several case studies in the near future. In addition, it will be contemplated the possibility of enriching the implemented procedure, allowing user to design core part, fixtures and vents in a semi-automatic way.

Funding Open access funding provided by Università degli Studi di Firenze within the CRUI-CARE Agreement.

Declarations

Conflict of interest The authors have no conflicts of interest to declare that are relevant to the content of this article. All authors certify that they have no affiliations with or involvement in any organization or entity with any financial interest or non-financial interest in the subject matter or materials discussed in this manuscript. The authors have no financial or proprietary interest in any material discussed in this article.

Open Access This article is licensed under a Creative Commons Attribution 4.0 International License, which permits use, sharing, adaptation, distribution and reproduction in any medium or format, as long as you give appropriate credit to the original author(s) and the source, provide a link to the Creative Commons licence, and indicate if changes were made. The images or other third party material in this article are included in the article's Creative Commons licence, unless indicated otherwise in a credit line to the material. If material is not included in the article's Creative Commons licence and your intended use is not permitted by statutory regulation or exceeds the permitted use, you will need to obtain permission directly from the copyright holder. To view a copy of this licence, visit <http://creativecommons.org/licenses/by/4.0/>.

References

1. Marker, S., Mohr, M., Østergaard, D.: Simulation-based training of junior doctors in handling critically ill patients facilitates the transition to clinical practice: an interview study. *BMC Med. Educ.* **19**(1), 1–8 (2019). <https://doi.org/10.1186/s12909-018-1447-0>
2. Aggarwal, R., Mytton, O.T., Derbrew, M., Hananel, D., Heydenburg, M., Issenberg, B., MacAulay, C., Morimoto, T., Soper, N., Ziv, A., Reznick, R.: Training and simulation for patient safety. *Qual. Saf. Health Care* **19**(2), 34–43 (2010). <https://doi.org/10.1136/qshc.2009.038562>
3. Singh, N., Shrivastava, P.: Recent advances and developments in the field of rapid prototyping for clinical applications. *Addit. Manuf. Med. Appl.* 137–149 (2022)
4. Rodr, E., Nifong, L.W., Jr.: Robotic mitral surgery at east Carolina university. *Int. J. Med. Robot. Comput. Assist. Surg.* **2**(3), 211–215 (2006). <https://doi.org/10.1002/rcs.80>
5. van der Meijden, O.A.J., Schijven, M.P.: The value of haptic feedback in conventional and robot-assisted minimal invasive surgery and virtual reality training: a current review. *Surg. Endosc.* **23**(6), 1180–1190 (2009). <https://doi.org/10.1007/S00464-008-0298-X>
6. Miyazaki, T., Yamasaki, N., Tsuchiya, T., Matsumoto, K., Takagi, K., Nagayasu, T.: Airway stent insertion simulated with a three-dimensional printed airway model. *Ann. Torac. Surg.* **99**(1), 21–23 (2015). <https://doi.org/10.1016/j.athoracsur.2014.10.021>
7. Cheng, G.Z., Estepar, R.S.J., Folch, E., Onieva, J., Gangadharan, S., Majid, A.: Three-dimensional printing and 3D slicer powerful tools in understanding and treating structural lung disease. *Chest* **149**(5), 1136–1142 (2016). <https://doi.org/10.1016/j.chest.2016.03.001>
8. Wilson, C.A., Arthurs, O.J., Black, A.E., Schievano, S., Hunt, C., Van Hoog, S., Wallis, C., Sury, M.R.J.: Printed three-dimensional airway model assists planning of single-lung ventilation in a small child. *Br. J. Anaesth.* **115**(4), 616–620 (2015). <https://doi.org/10.1093/bja/aev305>
9. Xu, C., Brennick, M.J., Dougherty, L., Wootton, D.M.: Modeling upper airway collapse by a finite element model with regional tissue properties. *Med. Eng. Phys.* **31**(10), 1343–1348 (2009). <https://doi.org/10.1016/j.medengphy.2009.08.006>
10. Safshekan, F., Tafazzoli-Shadpour, M., Abdouss, M., Shadmehr, M.B.: Mechanical characterization and constitutive modeling of human trachea: age and gender dependency. *Materials (Basel)* **9**(6), 456 (2016). <https://doi.org/10.3390/ma9060456>
11. Ozen, M., Sayman, O., Havitcioglu, H.: Modeling and stress analyses of a normal foot-ankle and a prosthetic foot-ankle complex. *Acta Bioeng. Biomech.* **15**(3), 19–27 (2013). <https://doi.org/10.5277/abb130303>
12. Puggelli, L., Uccheddu, F., Volpe, Y., Furferi, R., Di Feo, D.S.I.P.: Accuracy assessment of CT-based 3D bone surface reconstruction. *Lecture Notes in Mechanical Engineering*, pp. 487–496. (2019). https://doi.org/10.1007/978-3-030-12346-8_47
13. Santarelli, C., Puggelli, L., Carfagni, M., Governi, L.: Preliminary Study of a High-fidelity Simulator for the Management of Paediatric Tracheal Pathologies. *Lecture Notes in Mechanical Engineering*, pp. 773–784. (2022). https://doi.org/10.1007/978-3-030-91234-5_78
14. Smooth-on website. <https://www.smooth-on.com/products/dragon-skin-30/>
15. Halliday, N.L., Chung, H.M., Chung, K.W.: *Gross Anatomy*. Wolters Kluwer, Alphen AAN den Rijn (NL), (2019)
16. Santarelli, C., Puggelli, L., Volpe, Y., Serio, P., Furferi, R.: A Semi-automatic Procedure to Assist Physicians in Paediatric Airway Stenting. *Lecture Notes in Mechanical Engineering*, (in press)
17. Legland, D.: Geometric Computing Library for 3D Shapes: Meshes, Points, Lines, Planes, (2022). <https://www.mathworks.com/matlabcentral/fileexchange/24484-geom3d>
18. Bergström, P.: Toolbox for Working with IGES CAD-Models in MATLAB, (2022). <https://www.mathworks.com/matlabcentral/fileexchange/13253-iges-toolbox>
19. Douglas, D.H., Peucker, T.K.: Algorithms for the reduction of the number of points required to represent a digitized line or its caricature. *Int. J. Geogr. Inf. Geovisualiz.* **10**, 112–122 (1973). <https://doi.org/10.1002/9780470669488.ch2>
20. Delaunay, B.: Sur la sphere vide. *Bull. Acad. Sci. l'URSS Classe Sci. Math. Nat.* **6**, 793–800 (1934)

Publisher's Note Springer Nature remains neutral with regard to jurisdictional claims in published maps and institutional affiliations.